MATERIAL SPREADING AND COMPACTION IN POWDER-BASED SOLID FREEFORM FABRICATION METHODS: MATHEMATICAL MODELING

Yaser Shanjani and Ehsan Toyserkani
Department of Mechanical and Mechatronics Engineering, University of Waterloo, 200 University Avenue West Waterloo, ON N2L 3G1, Canada

Abstract
In this study, the spreading and compaction of powder by a counter-rotating roller, in the solid freeform fabrication (SFF) process, is modeled and characterized. The effect of layer thickness, roller diameter, amount of loose powder, and its initial density on the powder bed's relative density and roller compaction pressure is investigated.

Introduction

Density is a crucial characteristic of the parts fabricated by solid freeform fabrication (SFF). This factor directly affects the mechanical properties and functionality of the prototyped part. In powder-based SFF methods, such as 3D-printing and selective laser sintering (SLS), the density of the fabricated parts substantially depends on the density of the powder layers, which are sequentially spread and compacted by a counter-rotating rolling mechanism, as shown in Figure 1.
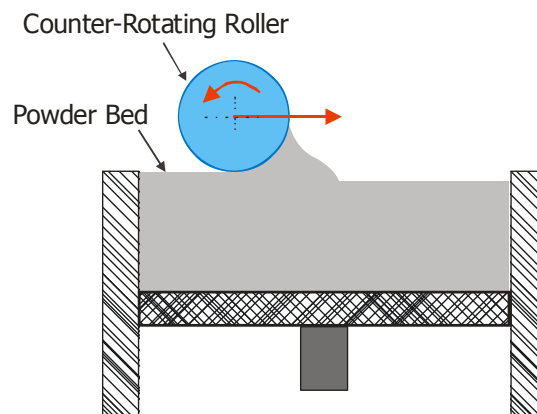

Figure 1: Schematic of powder spreading and compacting process by a counter-rotating roller

To arrive at the desired density in the powder bed, the parameters associated with the spreading mechanism (e.g., linear and rotational speed of the roller, roller surface properties, and powder layer thickness) must be carefully adjusted in such a way that an appropriate compaction force is applied on the powder bed by the roller. Since the properties of powder materials (e.g., spreadability and flowability) are inherently nonlinear, this optimization process is intricate.

The current efforts for obtaining the optimum properties of the spread powder layer are based on trial-and-error techniques, which must be carried out for any new powder material and characteristics. As an alternative approach, mathematical modeling provides insight to the compaction phenomenon. By using the mathematical modeling and simulation, engineers can

tune the process parameters for better control of the prototyped part's porosity. In spite of the apparent simplicity of the counter-rotating rolling compaction, there are too many unknown aspects of this process, from an analytical perspective.

Several investigations have been conducted on powder rolling and densification, and many theories have been developed to determine the material behavior in compaction conditions. Johanson [1] developed the first complex model for predicting the material flow undergoing continuous shear deformation between two rollers. The 1D slab method, in which the equilibrium force balance on a thin strip of material with a differential thickness is considered, has often been used to study the rolling, extrusion and drawing of metals [2]. Katashinskii et al. [3, 4] developed a mathematical model of the densification of powder by two rotating rollers, representing the stress-strain state of the powder being rolled in the densification zone. A complete review about this area of research is available in the literature [2].

This work is focused on the mathematical modeling of the powder compaction where a counter-rotating roller passes over the powder bed during the feeding step of the SFF process. Investigations are conducted to obtain the effect of the rolling parameters (layer thickness and roller diameter) on the kinematical characteristics of the process in the densification zone. The density and rolling contact pressure within the compacted powder bed are attained.

Mathematical Modeling

The parameters which are used in the following section are listed in Table 1, as the nomenclature.

Table 1: Nomenclature

Parameter	Description	parameter	Description
b	Slab length (m)	t_r	Shear stress between roller and loose powder (N/m^2)
e	Rate of densification (1/s)	α	Rolling angle (radian)
e_x	Rate of slab deformation in x direction (1/s)	α_{in}	Rolling upper bound (radian)
e_y	Rate of slab deformation in y direction (1/s)	δ	Slab width (m)
h	Slab height (m)	γ	Rate of shape change (1/s)
h_s	Powder layer thickness (m)	μ_p	Coefficient of friction between loose and compacted powder
m	Slab mass (kg)	μ_r	Coefficient of friction between roller and loose powder
n	Normal vector	Θ	Porosity
P	Hydrostatic stress (N/m^2)	Θ_i	Initial porosity
P_r	Roller contact pressure (N/m^2)	ρ	Density (kg/m^3)
$\bar{P}_r$	Roller contact pressure / σ_s	$\sigma_x, \sigma_y, \sigma_z$	Stress in x, y, and z directions (N/m^2)
Q	Reaction force (N)	$\bar{\sigma}_x$	Stress in x directions / σ_s
R	Roller radius (m)	σ_s	Yield stress of bulk material (N/m^2)
t_q	Shear stress between loose and compacted powder (N/m^2)	τ	Stress deviator (N/m^2)

The counter-rotating roller compaction of powder is analyzed with the 1D slab approach, for which some assumptions are taken into account. It is assumed that stress and strain vary only in the rolling direction and not in the width or thickness. Since the plastic strains are substantially higher than the elastic strain, the elastic deformations are negligible. In addition, body forces (gravitational forces) can be ignored in comparison with the frictional and compaction forces. In addition, it is assumed that the underneath powder layers are compacted enough so that the new layer of rolling powder is prepared onto a stationary plane plate.

The effects of roller rotational and linear motions speed are taken into account by the coefficient of the friction between the roller and powder. Since the material is prevented from spreading laterally during rolling, and the roller length is relatively larger than its diameter and powder layer thickness, the process is treated as a plane strain problem.

By considering a continuum mechanics for this process, similar to the phenomenon of the laminar flow of a viscous liquid, a steady flow of the powder takes place into the densification zone. The analysis is performed according to the plasticity theories for compressible porous solids.

For simplification, it is assumed that the power is spread and then compacted to a certain thickness. As shown in Figure 2, α_{in} determines the beginning angular position of the densification zone beyond where the compaction of the powder takes place. In other words, α_{in} represents the amount of powder which flows into the densification zone. The lowest rolling gap h_s, which is equal to powder layer thickness, occurs at α_{in} =0. The coefficient of friction between the roller surface and the powder is assumed to be constant on entire roller-powder contact area. This parameter depends on several factors, including the powder particle size and shape, roller surface smoothness, and roller rotational (ω) and linear (v) motion speed.
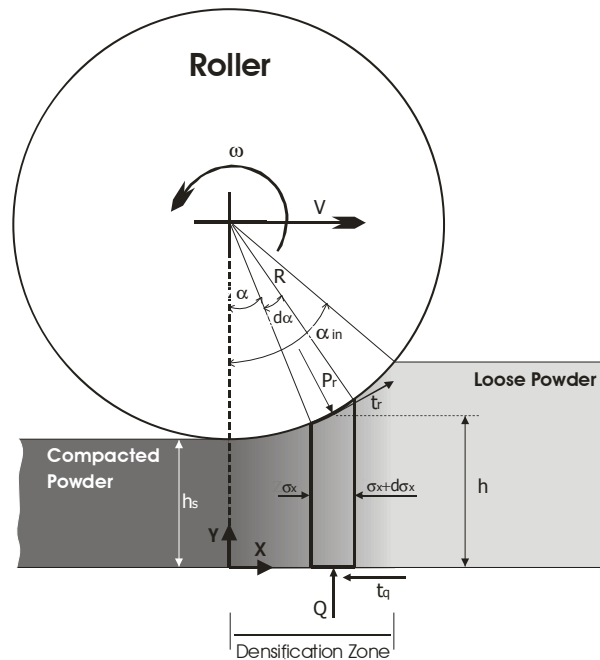

Figure 2: Forces and stresses acting on the powder densification zone

To derive the governing equations on the powder under the roller, a slab of powder with an infinitely small thickness is considered as shown in Figure 2. It is oriented perpendicular to the rolling direction and the applied forces. The stresses acting on the slab, the roll pressure P_r, and the shear stresses t_r and t_q, are also depicted in Figure 2. The equilibrium of the forces in the rolling direction, that is, the x-direction, for a unit length in the roll width, leads to the following expression:

$$\frac{d\sigma_x}{d\alpha} = \frac{R}{h} \cdot \left(P_r \cdot \sin\alpha + t_r \cdot \cos\alpha - t_q \right) \tag{1}$$

With the consideration of the equation of continuity, for a compressible material, the density is not constant and the continuity equation (mass conservation) is written as follows [3]:

$$m = h \cdot \rho \cdot \delta \cdot b \;\; \Rightarrow \;\; \frac{\dot{\delta}}{\delta} + \frac{\dot{h}}{h} + \frac{\dot{\rho}}{\rho} = 0 \tag{2}$$

The terms $\dfrac{\dot{\delta}}{\delta}$ and $\dfrac{\dot{h}}{h}$ are the rates of the slab deformation in the directions x and y, respectively. Thus,

$$e_x = \frac{\dot{\delta}}{\delta} \;\; and \;\; e_y = \frac{\dot{h}}{h} \tag{3}$$

For the plane deformation of compressible materials, the compatibility equations are presented in (4)-(6), which are derived in [5]. Equations (4) and (5) represent the load surfaces.

$$\frac{P^2}{\psi + \frac{1}{6} \cdot \phi} + \frac{\tau^2}{\frac{1}{2} \cdot \phi} = \frac{2}{3} \cdot (1 - \Theta) \cdot \sigma_s^2 \tag{4}$$

and

$$\frac{1}{2} \cdot P \cdot \phi \cdot \gamma = \tau \cdot \left(\psi + \frac{1}{6} \cdot \phi \right) \cdot e \tag{5}$$

$$\psi = \frac{2}{3} \cdot \frac{(1-\Theta)^2 \cdot (\Theta_i - \Theta)}{\Theta \cdot \Theta_i}; \qquad \phi = \frac{(1-\Theta) \cdot (\Theta_i - \Theta)}{\Theta_i} \tag{6}$$

P is the first invariant of the stress tensor, when τ is the modified second invariant of its deviator [5] such that

$$P = \frac{1}{3} \sigma_{ii} \;\; and \;\; \tau^2 = \left(\sigma_{ij} - P \cdot \delta_{ij} \right) \cdot \left(\sigma_{ij} - P \cdot \delta_{ij} \right) \tag{7}$$

The relation between the stress tensor and deformation rate tensor is written as

$$\sigma_{ij} = \beta \cdot \left(\phi \cdot e_{ij} + \left(\psi - \frac{1}{3} \cdot \phi \right) \cdot e \delta_{ij} \right) \;\; and \;\; e = e_{ij} \delta_{ij} \tag{8}$$

The stress in the third axis (along the roller length) is obtained in terms of σ_x and σ_y such that

$$\sigma_z = \frac{\psi - \frac{1}{3} \cdot \phi}{2 \cdot \psi + \frac{1}{3} \cdot \phi} \cdot (\sigma_x + \sigma_y) \tag{9}$$

As a result the first invariant P is

$$P = \frac{1}{2} \cdot (\sigma_x + \sigma_y) \tag{10}$$

According to Shtern [5], in powder rolling, when the angle of upper boundary of the densification zone does not exceed 0.15-0.20 radians, the following approximation is valid:

$$\sigma_1 = \sigma_y = P_r \text{ and } \sigma_3 = \sigma_x \tag{11}$$

Therefore, the term $4 \cdot \tau_{xy}^2$ can be neglected for τ , and then

$$\tau = \frac{1}{2} \cdot (\sigma_x - P_r) \tag{12}$$

Invariants γ and e are expressed in terms of the principal deformation rates as [3]

$$e = e_1 + e_2 \tag{13}$$
$$\gamma = |e_1 - e_2|$$

By applying (10)-(13), along with (5) e is found as

$$e = \frac{\frac{1}{2} \cdot \phi}{\psi + \frac{1}{6} \cdot \phi} \cdot \frac{\sigma_x + P_r}{\sigma_x - P_r} \cdot \left| \frac{\dot{\delta}}{\delta} - \frac{\dot{h}}{h} \right| \tag{14}$$

In addition, from (2), the following can be computed:

$$\frac{\dot{\delta}}{\delta} + \frac{\dot{h}}{h} = -\frac{\dot{\rho}}{\rho} \Rightarrow e = -\left(\frac{\dot{\rho}}{\rho} \right) \tag{15}$$

With (15) and the resultant expression for e in (14), the following relation is obtained:

$$\frac{\dot{\rho}}{\rho} = \frac{-2}{1 + \frac{\psi + \frac{1}{6} \cdot \phi}{\frac{1}{2} \cdot \phi} \cdot \frac{P_x - \sigma_x}{P_x + \sigma_x}} \cdot \frac{\dot{h}}{h} \tag{16}$$

From the geometry perspective, it is observed that $h = h(\alpha) = h_s + R \cdot (1 - \cos \alpha)$. Since the process is analyzed in the steady-state, ρ is only a function of α. Consequently,

$$\frac{d\rho}{d\alpha} = \frac{-2 \cdot \rho \cdot \sin \alpha}{\left(\dfrac{h_s}{R} + 1 - \cos \alpha\right) \cdot \left(1 + \dfrac{A^2}{B^2} \cdot \dfrac{P_r - \sigma_x}{P_r + \sigma_x}\right)} \tag{17}$$

where

$$A^2 = \frac{2}{3} \cdot \left(\psi + \frac{1}{6} \cdot \phi\right) \cdot (1 - \Theta); \quad B^2 = \frac{1}{3} \cdot \phi \cdot (1 - \Theta) \tag{18}$$

By substituting (7) in the load surface equilibrium (5), and solving it for P_r,

$$\bar{P}_r = \frac{A^2 - B^2}{A^2 + B^2} \cdot \bar{\sigma}_x + \frac{2 \cdot A \cdot B}{A^2 + B^2} \cdot \sqrt{A^2 + B^2 - \bar{\sigma}_x^2} \tag{19}$$

where $\bar{P}_r = \dfrac{P_r}{\sigma_s}$ and $\bar{\sigma}_x = \dfrac{\sigma_x}{\sigma_s}$ are the dimension-less stress components.

In addition, the ordinary differential equation, obtained from the force equilibrium, is

$$\tag{20}$$

$$\frac{d\bar{\sigma}_x}{d\alpha} = \frac{P_r}{\left(\dfrac{h_s}{R} + 1 - \cos \alpha\right)} \cdot \left(\sin \alpha + \mu_f \cdot \cos \alpha - \mu_p \cdot (\cos \alpha - \mu_f \cdot \sin \alpha)\right) \tag{20}$$

by considering $t_r = \mu_r \cdot P_r$ and $t_q = \mu_p \cdot Q = \mu_p \cdot P_r \cdot (\cos \alpha - \mu_r \cdot \sin \alpha)$.

Equations (17) and (20) form a governing equations system of the compaction process. By adjusting the initial values for the α_{in}, coefficients of friction μ_p and μ_r, initial density of powder $\rho_{initial}$, layer thickness (rolling gap) h_s, and roller radius R, and by using a numerical algorithm of Euler developed in MATLB, the roller contact pressure, stress distributions, and density gradient of the powder along the rolling direction are obtained.

Results and Discussion

The derived governing equations are calculated for a wide range of boundary conditions and initial values which are based on the actual conditions for the part fabrication with the available SFF machines. Table 2 lists the analysis parameters and subjected values.

Table 2: Analysis parameters

Parameter	Value	Description
μ_p	0.5	Friction coefficient of loose powder and underlying compacted powder layer
μ_r	0.3	Friction coefficient of roller-powder contact area
R	10mm	Roller radius
$\rho_{initial}$	30%	Powder initial density
α_{in}	0.2rad	Upper-bound of rolling angle

The relative density (RD) of the compacted powder layer is defined as

$$RD = \frac{bulk\ density\ of\ compacted\ powder}{powder\ material\ density} \quad (21)$$

The variation of RD in relation to the changes in the powder layer thickness, h_s, is shown in Figure 3. The plot is represented as a function of the rolling angle α, which varies from α_{in} (the upper-bound) to zero, along the densification zone. The selected layer thicknesses are accessible in a typical 3D-printing machine. Also, the powder relative density corresponding to the layer thicknesses is plotted in Figure 4, for different α_{in}. The value of α_{in} represents the amount of powder which is trapped into the densification zone and indirectly depends on several factors, such as the flowability of powder and roller-powder coefficient of friction. It can be seen that the larger the thickness, the lower the RD in the compacted powder. It is obvious that RD increases with α_{in}. For a constant α_{in}, higher h_s means less percentage of loose powder is compacted which, in turn, results in a lower density in the compacted powder. However, if we assume the percentage of the compacted powder to be constant (x), α_{in} functions with h_s as $\alpha_{in} = ArcCos(1 - \frac{x \times h_s}{R})$, and RD varies along the densification zone as illustrated in Figure 5.
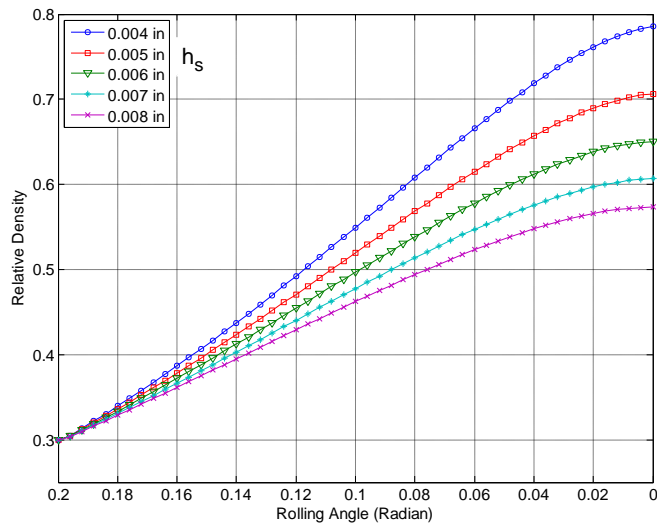
Figure 3: Effect of the powder layer thickness on the relative density distribution along the densification zone for $\alpha_{in} = 0.2\,rad$
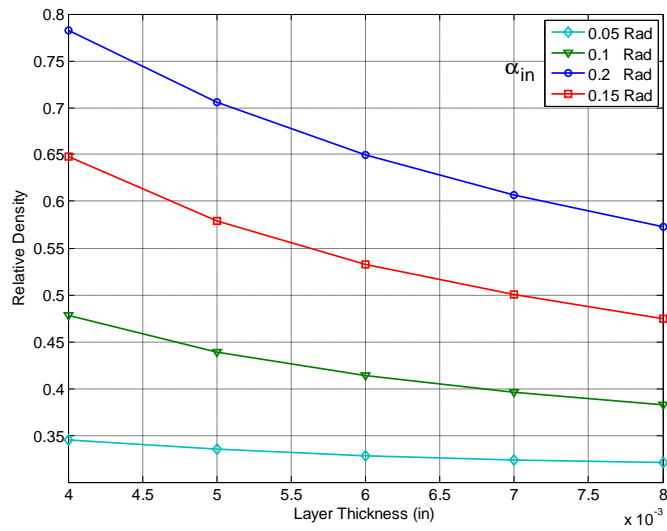

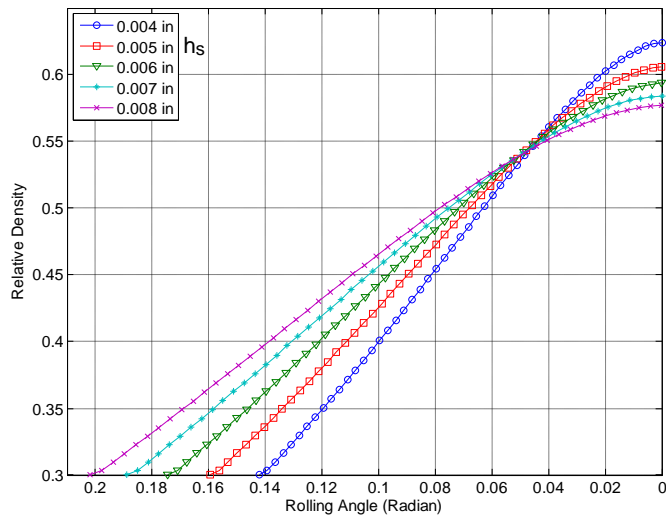Figure 4: Relative density of compacted powder layer vs. the adjusted layer thickness

Figure 5: Effect of the powder layer thickness on the relative density distribution along the densification zone

The RD varies due to the changes that occur in the longitudinal strain, whereas the vertical strain is unchanged in the slab element. As a result, according to the law of mass conservation, (2), the relative density rises.

The upper-bound of the rolling angles, α_{in}, varies in relation to the amount of powder in front of the roller. It is obvious that providing more powder to be conveyed into the densification zone, for a constant h_s, results in a denser compacted layer. Figure 6 shows this effect for h_s =0.005in.
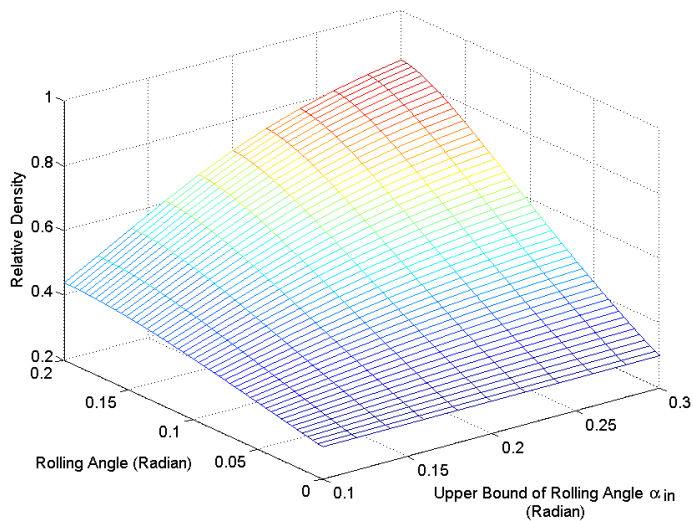

Figure 6: Effect of the upper-bound of the rolling angle on the relative density distribution along the densification zone for $h_s = 0.005in$

The data from the experimental investigations of other researchers [4] show that the distribution of the powder density in the densification zone depends on two factors: the absolute and relative magnitudes of the longitudinal and normal stresses, and the geometry of the deformation zone. The distribution of the roller normal contact pressure along the densification zone in the powder layer is graphed in Figure 7. It is obvious that the maximum compact pressure occurs in the narrowest gap between the roller and the underneath powder layer, that is, at the rolling angle of zero. The contact pressure decreases by choosing the larger powder layer thickness.
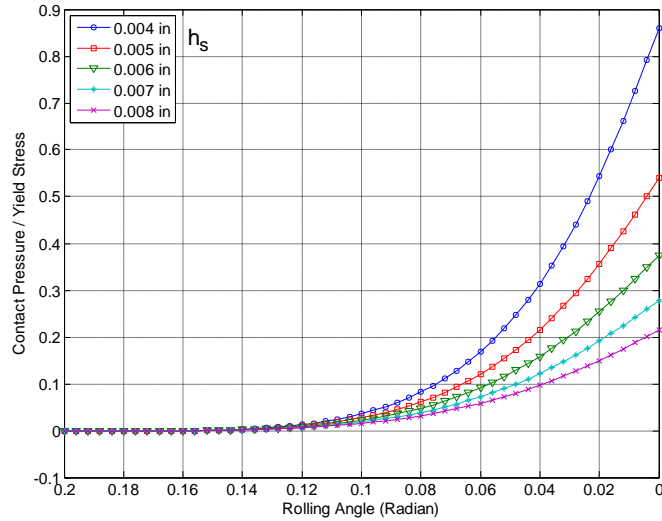

Figure 7: Effect of the powder layer thickness on the contact pressure distribution along the densification zone

By keeping all the parameters unchanged, an increase in the apparent density of the starting powder (initial density) results the increase in the relative density of the compacted layer. However, the amount of this increase depends on the initial densities. The percentage of the RD change for different initial densities is presented in Figure 8. It is observed that the powder with a lower initial density shows a higher change in RD.
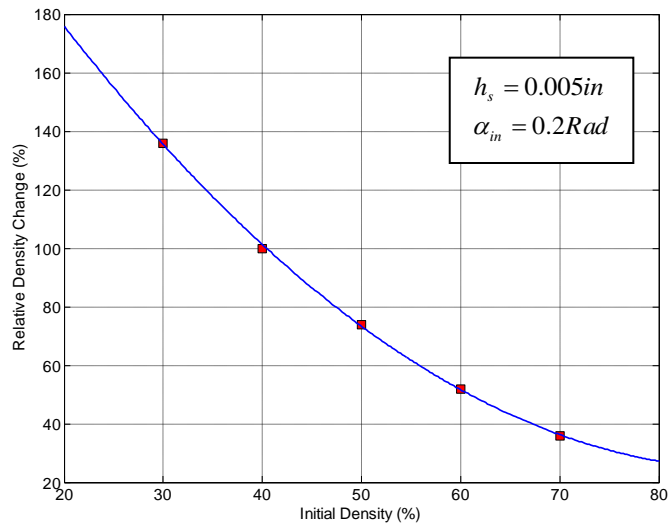
Figure 8: Relative density changes vs. initial apparent density of powder

The diameter of the roller has also a crucial influence on the powder compaction. Providing the constant amount of the powder to convey into the densification zone, by properly adjusting the α_{in}, the RD of the powder layers can be tailored using the rollers with different diameters. The effect is shown in Figure 9.
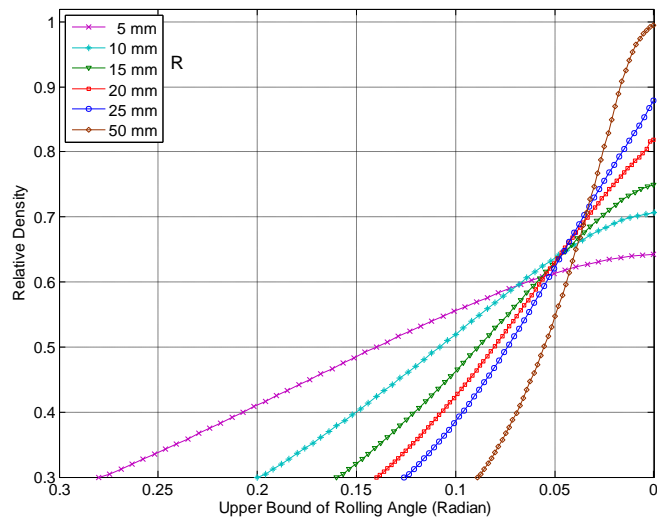

Figure 9: Effect of roller diameter on the on the relative density distribution along the densification zone

The results are useful in estimating the relative density of the parts, fabricated by the SFF methods, such as 3D-printing and SLS that use a counter-rotating roller for the powder spreading. In addition, (17) to (20) can be solved for the inverse problem. Therefore, to fabricate a part with a specific density, the requisite layer thickness, roller diameter, and powder condition (initial apparent density and particle size) can be chosen based on either of the graphs or solving

the reverse problem. It is noteworthy that the minimum and maximum values for the layer thickness and rolling velocity are restricted for any method of SFF.

Conclusions

A one-dimensional mathematical modeling of powder compaction by a counter-rotating roller was conducted. The density distribution in the powder bed along the densification zone, in the rolling direction, was analyzed. It was shown that how the layer thickness, roller geometry, and initial powder properties affect on the compacted powder relative density, which directly yields to the properties of the prototyped part. In the future work, the model will be enhanced and validated through experiments.

References

[1] J. R. Johanson, "A rolling theory for granular solids," *ASME, Journal of Applied Mechanics,* vol. 32, ser. E, pp. 842-848, 1965.

[2] J. C. Cunningham, "Experimental studies and modeling of the roller compaction of pharmaceutical powders," *Derexel University,* pp. 13, 2006.

[3] V. P. Katashinskii and M. B. Shtern, "Stress-strain state of powder being rolled in the densification zone, I. Mathematical model of rolling in the densification zone ," *Powder Metallurgy and Metal Ceramics,* vol. 11(251), pp. 17-21, 1983.

[4] V. P. Katashinskii and M. B. Shtern, "Stress-strain state of powder being rolled in the densification zone, II. Distribution of density, longitudinal strain, and contact stress in the densification zone," *Powder Metallurgy and Metal Ceramics,* vol. 12(252), pp. 9-13, 1983.

[5] M. B. Shtern, "Plane deformation characteristics of compressible materials," *Powder Metallurgy and Metal Ceramics,* vol. 3(231), pp. 14-21, 1982.